J. Appl. Cryst. (1998). **31**, 718–725

Refinement of the Ferri- and Paramagnetic Phases of Magnetite from Neutron Multiple Diffraction Data

V. L. Mazzocchi* and C. B. R. Parente

Instituto de Pesquisas Energéticas e Nucleares, Comissão Nacional de Energia Nuclear, CP 11049 Pinheiros, 05422-970 São Paulo, SP, Brazil. E-mail: vlmazzo@curiango.ipen.br

(*Received 27 December 1996; accepted 20 March 1998*)

Abstract

Structural parameters for the ferrimagnetic and paramagnetic phases of magnetite have been refined from neutron multiple diffraction data. Experimental neutron multiple diffraction patterns were obtained by measuring the 111 primary reflection of a natural single crystal of this compound. Measurements were made at room temperature for the ferrimagnetic phase and at 976 K for the paramagnetic phase. The corresponding simulated patterns have been calculated by *MULTI*, a computer program for the simulation of neutron multiple diffraction patterns. A step-by-step process was used in the refinements according to the parameter-shift method. Both isotropic and anisotropic thermal parameters were assumed for the temperature factor. Isotropic thermal parameters were considered in two different ways: an overall parameter for all ions in the structure and three different parameters for the three special positions occupied by them in the structure. The best results were found in the refinements with anisotropic thermal parameters. In this case, the values of the profile *R* factor found for these refinements were 3.00 and 3.32%, respectively, for the ferrimagnetic and paramagnetic phases.

1. Introduction

Recently, Mazzocchi & Parente (1994) studied the β phase of quartz employing neutron multiple diffraction (NMD) as a method of analysis. Simulated patterns for an ordered and a disordered model of the β-quartz structure were calculated by *MULTI*, a computer program for the simulation of NMD patterns. *MULTI* uses the approximate intensity solutions derived by Parente *et al.* (1994) for a many-beam case. A Gaussian function was assumed for the mosaic spread distribution of the crystal. Although no refinement had been done in the analysis, experimental and simulated pattterns showed a rather good agreement.

In this work, the ferri- and paramagnetic phases of magnetite are refined from NMD data. Experimental NMD patterns were measured with a natural single crystal of magnetite, at room temperature for the ferrimagnetic phase and at 976 K for the paramagnetic phase. Details are given of the crystal and magnetic structures of magnetite, the experimental procedures, the process of refinement and the results obtained.

2. Crystal and magnetic structures of magnetite

According to Verwey and co-workers (Verwey & de Boer, 1936; Verwey & Haayman, 1941; Verwey & Heilmann, 1947; Verwey *et al.*, 1947), above *circa* 119 K magnetite (Fe_3O_4) is an inverse Fe spinel $Fe^{3+}(Fe^{2+}Fe^{3+})O_4^{2-}$. The inverse spinel structure of magnetite has a large unit cell containing eight Fe^{3+} ions in tetrahedral *A* sites and eight Fe^{2+} plus the remaining eight Fe^{3+} ions in octahedral *B* sites. Ions in magnetite are distributed in the following positions of the space group $Fd\bar{3}m$, the origin being taken at the center ($\bar{4}3m$), $-1/8$, $-1/8$, $-1/8$ from the centre ($\bar{3}m$). O^{2-} in 32(*e*): x, x, x; Fe^{2+} and Fe^{3+} in equal numbers and random distribution in 16(*d*): 5/8, 5/8, 5/8; Fe^{3+} in 8(*a*): 0, 0, 0.

In an ideal spinel structure x is equal to 3/8 (0.375), the arrangement of the O^{2-} ions equalling exactly a cubic close packing. In an actual spinel structure the packing is, in general, slightly distorted and x differs from 3/8. In the inverse spinel structure of magnetite, as well as in many other spinel-like structures, x slightly exceeds 3/8 causing a distortion in the close packing of the O^{2-} ions (Verwey & Heilmann, 1947).

The magnetic structure of magnetite, at room temperature, is of the type Néel *A*–*B*. Néel (1948), accounting for the observed magnitude of the saturation magnetic moment, which could only result from the ferrous ions alone, postulated that the ions on the *A* sites in magnetite were coupled antiferromagnetically to those on the *B* sites. In such a coupling, in fact, the contribution of the ferric ions is null since they are distributed in equal numbers on both *A* and *B* sites. On the other hand, the contribution of the ferrous ions is maximal, since all of them are on the *B* sites. This ferrimagnetic structure of magnetite was confirmed by Shull *et al.* (1951) using neutron powder diffraction data in the analysis. Above the Curie temperature, *circa* 853 K, magnetite is magnetically disordered, *i.e.* it is a paramagnet.

ISSN 0021-8898

3. Experimental

The measurements were performed on the Instituto de Pesquisas Energéticas e Nucleares multipurpose neutron diffractometer, installed at the IEA-R1 2 MW research reactor, São Paulo, Brazil. On this instrument, the Soller collimator for the monochromatic beam (λ = 1.137 Å) is substituted by a special collimator which limits both horizontal and vertical beam divergences to about 10′. A five-circle goniometer is used to perform the φ scans (Mazzocchi & Parente, 1994). The NMD measurements were carried out with a natural crystal of magnetite of unknown purity. The crystal has an irregular shape with a volume of about 5 cm^3. It was previously oriented in the neutron beam in order to find roughly one of its [111] directions.

To heat the crystal, an appropriate cylindrical resistance furnace was mounted in the φ axis. The furnace is the same as that used by the authors in the study of β-quartz (Mazzocchi & Parente, 1994). For this work, both the resistance and sustaining powder were substituted with more appropriate materials. The shape of the resistance was also modified. A nickel–chromium wire was first wound to form a helical resistance. In order to avoid the application of an alternating magnetic field over the crystal, the helical resistance was placed inside the furnace zigzagging through proper alumina insulators near the internal cylindrical surface. The crystal was fixed in the centre of the furnace with the previously oriented ⟨111⟩ direction nearly parallel to the φ axis. Well compacted alumina powder was used in order to keep the crystal in a stable position inside the furnace. Alumina produces a low background level and has a low absorption coefficient for neutrons. No Bragg peak of alumina was found to coincide with the reflection 111 of magnetite. A goniometer head linked the furnace to the φ axis permitting orientation of the crystal in the neutron beam.

The measurements were carried out after a careful orientation of the 111 primary reflection. For both phases, multiple diffraction data were taken with the crystal inside the furnace. For the high-temperature measurements, a variable transformer was used to energize the furnace and a strip-chart recorder to monitor the temperature. To avoid any cracking in the crystal, the voltage was slowly increased till the crystal reached a temperature well above the transition. The temperature stabilized at 976 K. We assumed that, at this temperature, the crystal was wholly in the paramagnetic phase.

Below the transition, the 111 reflection in magnetite is almost entirely due to the coherent magnetic scattering and is very strong. The contribution of the coherent nuclear scattering is very small. Above the transition, owing to the random orientation of magnetic moments, the coherent magnetic scattering vanishes and the 111 reflection is reduced to solely the contribution of the coherent nuclear scattering (Shull *et al.*, 1951). According to the intensity of the primary beam, below the transition temperature an *Aufhellung* pattern is obtained. Above it, the pattern becomes of the *Aufhellung–Umweg* type (Mazzocchi & Parente, 1994).

The φ scans were carried out in steps of 0.1°, 5 min of counting time each step, over an azimuthal angular interval extending from 0 to 83.5° for both patterns. Complete 60° patterns were obtained in this interval. This is in accordance with the existence of three-fold symmetry axes along the [111] directions in the cubic system (Chang, 1984). Since half of a 60° pattern is a mirrored image of the other half (Mazzocchi & Parente, 1994), the halves were summed to form a 30° pattern with double intensity.

4. Process of refinement

A process based on the parameter-shift method (Buhiya & Stanley, 1963) was employed in the refinements of the structural parameters. In the process, a first parameter is varied in steps large enough to provide variation of an R factor, while other parameters are maintained with fixed values. The interval of variation is appropriate for determining a minimum value for R ($R_{\min}$). The first parameter is then shifted to the value which gives $R_{\min}$ and a second parameter is in turn treated in the same way. The process continues until the last parameter is refined, completing a cycle of refinement. More than one cycle is, in general, necessary to ensure the convergence of the refinement. Clearly, the $R_{\min}$ found for the last parameter, in the last cycle, is the R factor for the refinement and the set of parameters is the result of the refinement as well.

The R factor used in this work is similar to the profile R factor of Rietveld (1969), used by him to evaluate the agreement between profiles. It is given by

$$R = \sum_k |I_k(\text{obs}) - cI_k(\text{calc})| / \sum_k I_k(\text{obs})$$

where I_k(obs) and I_k(calc) are, respectively, observed and calculated intensities in the kth azimuthal position; c is a scale factor which is varied in order to minimize R for each value assumed for a certain parameter in its interval of variation.

The refinements were done on a point-to-point basis, *i.e.* for each I_k(obs) a corresponding I_k(calc) was calculated by *MULTI* using a given set of structural parameters. Nuclear scattering amplitudes of 0.96 and 0.58 × 10^{-12} cm were used in the calculations for iron and oxygen, respectively, and magnetic scattering amplitudes of 1.08 and 1.35f × 10^{-12} cm for Fe^{2+} and Fe^{3+}, respectively (Hamilton, 1958). Similarly to the procedure adopted by Hamilton (1958), when studying the cubic and orthorhombic phases of magnetite, the form factor f for both types of ions was assumed to be equal to

Table 1. *Lattice, positional and thermal parameters found in the refinements of the ferrimagnetic phase of magnetite compared with refinements 4 and 6 of Fleet (1986)*

At the bottom of the table are values of the experimental parameters, scale factor (c) and refined mosaic spread (η). The values of the R factor found in the refinements are also listed.

Special positions	Parameters	Fleet (1986)		This work		
		Refinement 4	Refinement 6	Refinement I	Refinement II	Refinement III
	a (Å)	8.3985 (5)	8.3985 (5)	8.401 (0)	8.402 (0)	8.399 (6)
	B (Å^2)			1.15 (0)		
8(a)	B_a (Å^2)				0.90 (0)	
	β_{11} (Å^2)	0.348 (11)	0.339 (16)			0.28 (0)
16(d)	B_d (Å^2)				1.1 (3)	
	β_{11} (Å^2)	0.465 (11)	0.469 (6)			0.63 (5)
	β_{12} (Å^2)	0.048 (3)	0.052 (3)			0.27 (5)
32(e)	x	0.37968 (8)	0.37987 (6)	0.370 (5)	0.370 (0)	0.370 (7)
	B_e (Å^2)				1.3 (0)	
	β_{11} (Å^2)	0.541 (18)	0.550 (9)			0.07 (7)
	β_{12} (Å^2)	−0.044 (2)	−0.031 (9)			0.00 (8)
	η (rad)					0.0062 (6)
	c ($\times 10^5$)			1.620	1.630	2.285
	R (%)	2.2	2.2	3.99	3.96	3.00

that found by Corliss *et al.* (1953) for Fe^{3+} in magnesium ferrite. Since Fe^{2+} and Fe^{3+} occupy the 16(d) positions in equal numbers and in a random distribution, the magnetic scattering amplitude for these ions in such positions was calculated as the arithmetic mean of the amplitudes of Fe^{2+} and Fe^{3+}. The linear absorption coefficient of magnetite was calculated according to the formula

$$\mu = \rho_{Fe_3O_4}[\omega_{Fe}(\mu/\rho)_{Fe} + \omega_O(\mu/\rho)_O]$$

where $\rho_{Fe_3O_4}$ is the density of solid magnetite, ω_{Fe} and ω_O are the proportions by weight of iron and oxygen in magnetite, and $(\mu/\rho)_{Fe}$ and $(\mu/\rho)_O$ are the mass absorption coefficients for these elements (Bacon, 1975). The following values were used in the calculations: $\rho_{Fe_3O_4} = 5.1974$ gcm^{-3}, $\omega_{Fe} = 0.72$, $\omega_O = 0.28$, $(\mu/\rho)_{Fe} = 0.015$ cm^2 g^{-1} and $(\mu/\rho)_O = 0.00001$ cm^2 g^{-1}. With these values μ was found to equal 0.056 cm^{-1}.

The initial values of a and x, used to begin the ferrimagnetic phase refinements, were found from the work of Fleet (1986). In a first refinement (I), an overall isotropic thermal parameter B was assumed for all ions in the structure. In a second refinement (II), different isotropic parameters were assumed for the special positions in the space group. They are denoted by B_a, B_d and B_e for the positions 8(a), 16(d) and 32(e), respectively. Finally, anisotropic thermal parameters were assumed in a third refinement (III). According to the point symmetry of the special positions (*International Tables for X-ray Crystallography*, 1976), the anisotropic thermal parameters for magnetite are reduced to $\beta_{11} = \beta_{22} = \beta_{33}$ and $\beta_{12} = \beta_{13} = \beta_{23}$ for Fe^{3+} in 8(a), Fe^{2+}/Fe^{3+} in 16(d) and O^{2-} in 32(e). In particular, for Fe^{3+} in 8(a) $\beta_{12} = \beta_{13} = \beta_{23} = 0$. Using the relationships given by Trueblood (1956), in order to transform the thermal parameters according to the symmetry

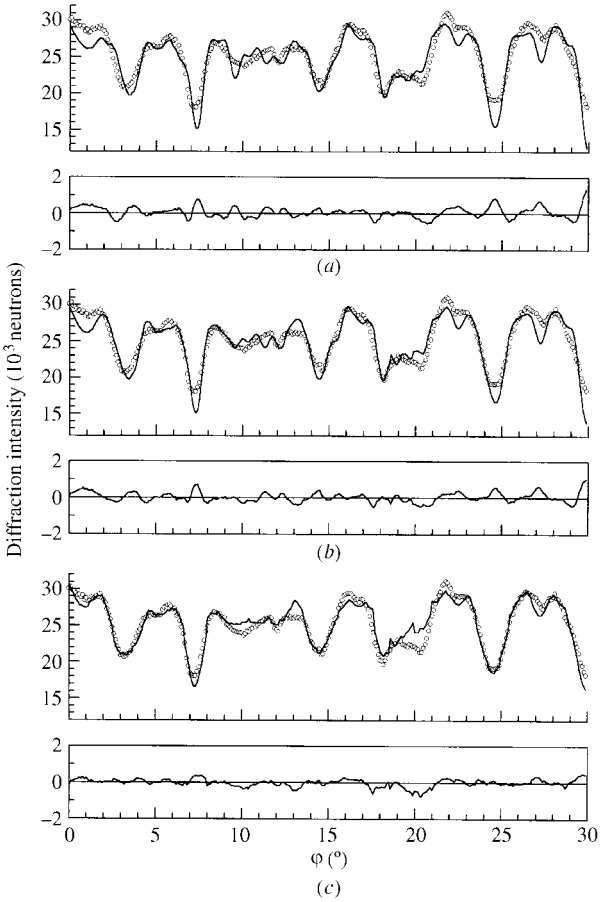

Fig. 1. Comparisons between the experimental NMD pattern obtained for the ferrimagnetic phase of magnetite and simulated patterns after refinements I (*a*), II (*b*) and III (*c*).

operations in the space group, and taking into account the above reductions, a pair β_{11}, β_{12} was determined for each ion in the structure. In refinements I and II, the standard deviation of the Gaussian distribution (η), assumed in the simulations by *MULTI*, was kept constant. Values of η, also called the mosaic spread of the distribution (Chang, 1984), were obtained from rocking curves of the 111 reflection of magnetite, measured at room temperature and at 976 K for the ferri- and paramagnetic phases, respectively. Both rocking curves gave the same value, namely 0.0044 rad. In refinement III, η was refined together with the structural parameters, taking as an initial value that indicated above.

5. Refinement of the ferrimagnetic phase

Refinements I, II and III, for the ferrimagnetic phase, were done in accordance with the process outlined in the preceding section. The results of such refinements are listed in Table 1, together with results of refinements 4 and 6 of Fleet (1986), for comparison. Refinements 4 and 6 were selected from others because of the following similarities between his and our results: (i) data were obtained with a natural single crystal of magnetite; (ii) although not entirely eliminated, systematic errors due to secondary extinction and simultaneous reflections were reduced in the data-sets for refinements 4 and 6; (iii) refinements 4 and 6 favour the centrosymmetric $Fd3m$ space group instead of the noncentrosymmetric $F\bar{4}3m$.

In Fig. 1, the experimental NMD pattern of the ferrimagnetic phase is compared with simulated patterns calculated by *MULTI*, with the final sets of parameters found in the refinements I, II and III [comparisons (*a*), (*b*) and (*c*), respectively]. Fig. 1 also shows the corresponding difference patterns obtained by calculating $w_k[I_k(\text{obs}) - cI_k(\text{calc})]$, where the weighting factor is given by $w_k = I_k(\text{obs})^{-1/2}$. A qualitative evaluation of the comparisons shows that (*c*) clearly shows the best agreement whereas the differences between (*a*) and (*b*) are almost negligible. Values of R in Table 1 confirm the above assertions. As an illustration of the high density of secondary reflections in the patterns, Fig. 2 shows part of the ferrimagnetic pattern indexed by *MULTI*. A count of secondary reflections per degree in the interval reveals that the density varies from a minimum of five reflections per degree, between 11 and 12°, to a maximum of 18, between 7 and 8°.

6. Refinement of the paramagnetic phase

Fig. 3 is the equivalent of Fig. 1 for the paramagnetic phase. Unlike Fig. 1, a comparison between refinements

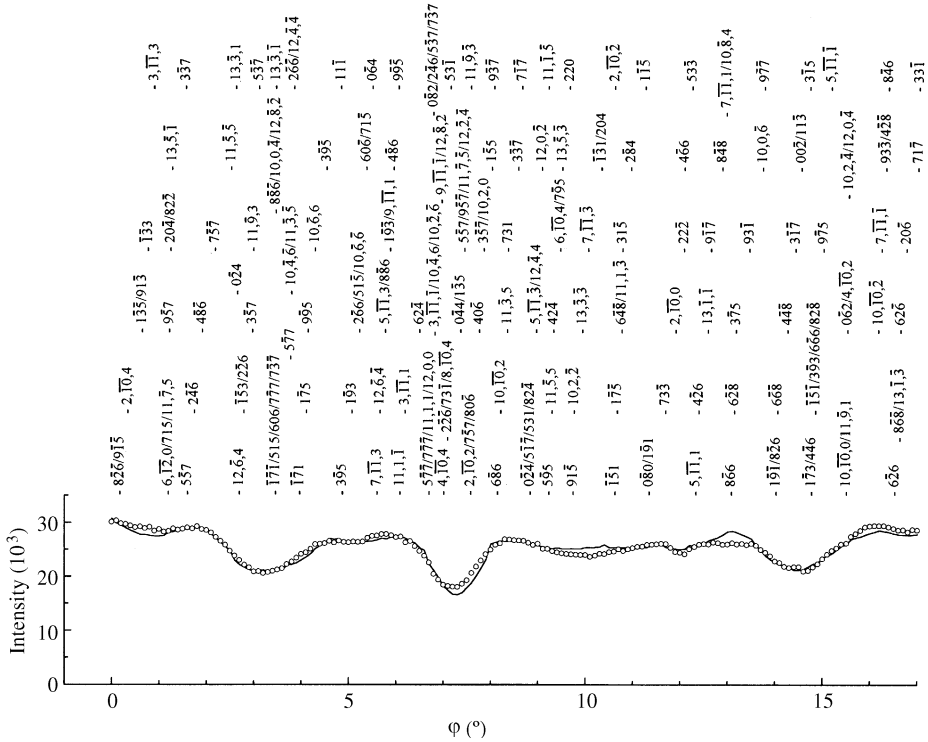

Fig. 2. Indexing of part of the NMD pattern for the ferrimagnetic phase of magnetite. Both experimental and simulated patterns are shown. A remarkable high density of secondary reflections is observed in the figure.

I, II and III [(*a*), (*b*) and (*c*) respectively] shows no remarkable differences. In fact, the values of *R* listed in Table 2 vary little, although they diminish from refinement I to III. Fig. 4 shows part of the NMD pattern of the paramagnetic phase indexed by *MULTI*. In this case, the density varies from six secondary reflections per degree, between 9 and 10 as well as 13 and 14°, to 18, between 8 and 9°. A comparison with Fig. 2 shows remarkable changes in the positions of most of the secondary reflections. This is, of course, a consequence of the increase in the cell parameter *a* owing to the increase in the temperature. [As a reference for this change in azimuthal positions see Cole *et al.* (1962)].

To verify the consistency of the values of *a* found for the paramagnetic phase in refinements I, II and III, its variation with temperature was calculated. The coefficients of linear expansion for magnetite, determined by Sharma (1950) for temperatures below and above the transition, were used in the calculations. According to this author, such coefficients are given by

$$\alpha_T = 8.417 \times 10^{-6} + 4.051 \times 10^{-9} T + 4.146 \times 10^{-11} T^2 \text{ for } T < T_C$$

$$\alpha_T = 7.674 \times 10^{-6} + 1.235 \times 10^{-9} T + 4.029 \times 10^{-11} T^2 \text{ for } T > T_C$$

where T_C is the transition temperature (Curie-point temperature). On the other hand, it is well known that the coefficient of linear expansion of a material is given by

$$\alpha_T = L_0^{-1}\, \mathrm{d}L/\mathrm{d}T$$

where L_0 is the value of a linear dimension at some temperature T_0 and $\mathrm{d}L$ is the increase of such a dimension when the temperature increases by $\mathrm{d}T$.

In this work, dimension L is the cell parameter a of magnetite. Then, substituting a by L and integrating, the variation of a as a function of the temperature increase is

$$a = a_0(1 + \alpha'_T \Delta T)$$

where

$$\alpha'_T = 8.417 \times 10^{-6} + 2.0255 \times 10^{-9} \Delta T + 1.3820 \times 10^{-11} \Delta T^2 \text{ for } T < T_C$$

$$\alpha'_T = 7.674 \times 10^{-6} + 0.6175 \times 10^{-9} \Delta T + 1.3430 \times 10^{-11} \Delta T^2 \text{ for } T > T_C$$

and $\Delta T = T - T_0$. These formulae allow the calculation of the cell parameter a at any temperature T given its value a_0 at a temperature T_0.

Fig. 5 shows the variation of a with temperature, calculated according to the formulae derived above. The value of a_0 used in the calculations is that found in refinement II for the ferrimagnetic phase, namely 8.402 Å. It is shown as a downward-pointing triangle at 303 K. The values obtained in refinements I and III, as well as those obtained in refinements I, II and III for the paramagnetic phase are also shown in Fig. 5. A few other values found in the literature for the ferrimagnetic phase (Tombs & Rooksby, 1951; Abrahams & Calhoun, 1953; Yoshida & Iida, 1979) are included in Fig. 5, for comparison. They are represented by open circles.

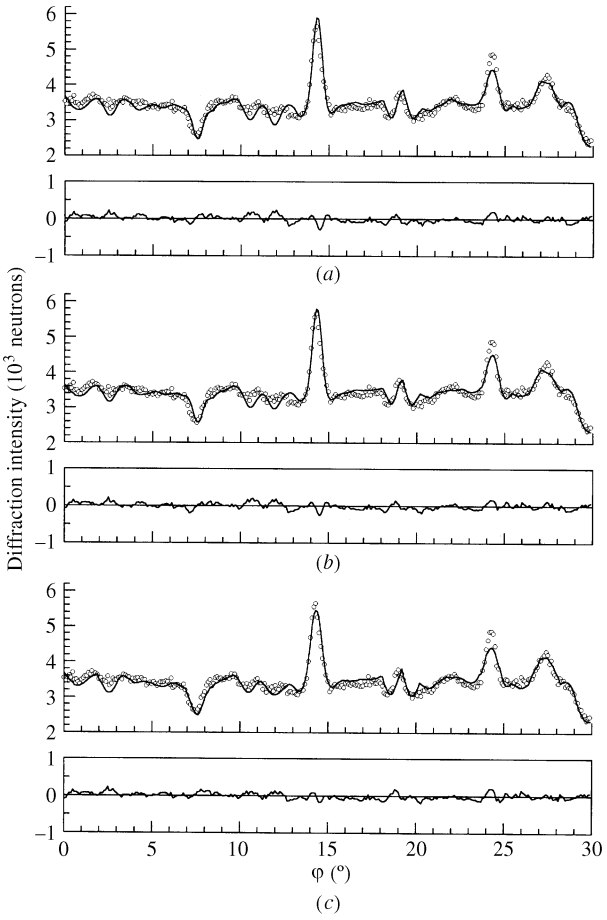

Fig. 3. Comparisons between the experimental NMD pattern obtained for the paramagnetic phase of magnetite and simulated patterns after refinements I (*a*), II (*b*) and III (*c*).

7. Discussion

Except for the positional parameter x, whose values found in the refinements of the ferrimagnetic phase are lower than 3/8, when they should be greater, the parameters refined for this phase are comparable with those found in the refinements 4 and 6 of Fleet (1986). A simple comparison between our and his results in Table 1 confirms this assertion. Concerning the paramagnetic

Table 2. *Lattice, positional and thermal parameters found in the refinements of the paramagnetic phase of magnetite*

At the bottom of the table are values of the experimental parameters, scale factor (c) and refined mosaic spread (η). The values of the R factor found in the refinements are also listed.

Special positions	Parameters	Refinement I	Refinement II	Refinement III
	a (Å)	8.486 (0)	8.490 (5)	8.491 (3)
	B (Å^2)	1.42 (5)		
8(a)	B_a (Å^2)		1.8 (5)	
	β_{11} (Å^2)			0.26 (0)
16(d)	B_d (Å^2)		1.1 (5)	
	β_{11} (Å^2)			0.41 (0)
	β_{12} (Å^2)			−0.00 (9)
32(e)	x	0.381 (5)	0.381 (5)	0.381 (7)
	B_e (Å^2)		1.8 (0)	
	β_{11} (Å^2)			0.19 (8)
	β_{12} (Å^2)			0.18 (3)
	η (rad)			0.0051 (2)
	c ($\times 10^5$)	2.040	1.995	2.380
	R (%)	3.56	3.46	3.32

phase, no crystallographic data were found in the literature for comparison with ours. Nevertheless, Fig. 5 shows that, at least, parameter a is consistent with the value calculated in accordance with Sharma (1950). It should be noted that, for this phase, x was greater than 3/8 as expected.

It is worth mentioning that Fleet (1986) pointed out the enhancement of weak and *Fd*3*m*-forbidden reflections as an effect of multiple diffraction. Another source of errors, according to Fleet, is the occurrence of secondary extinction. Clearly, in this work, multiple diffraction is not a disturbing effect. It is, in fact, the essence of the method employed in the structural analysis performed here. On the other hand, secondary extinction which is, in general, a very intense phenomenon in neutron diffraction was not a problem. Indeed, the program used for the simulations (*MULTI*) calculates intensities by using approximate solutions that

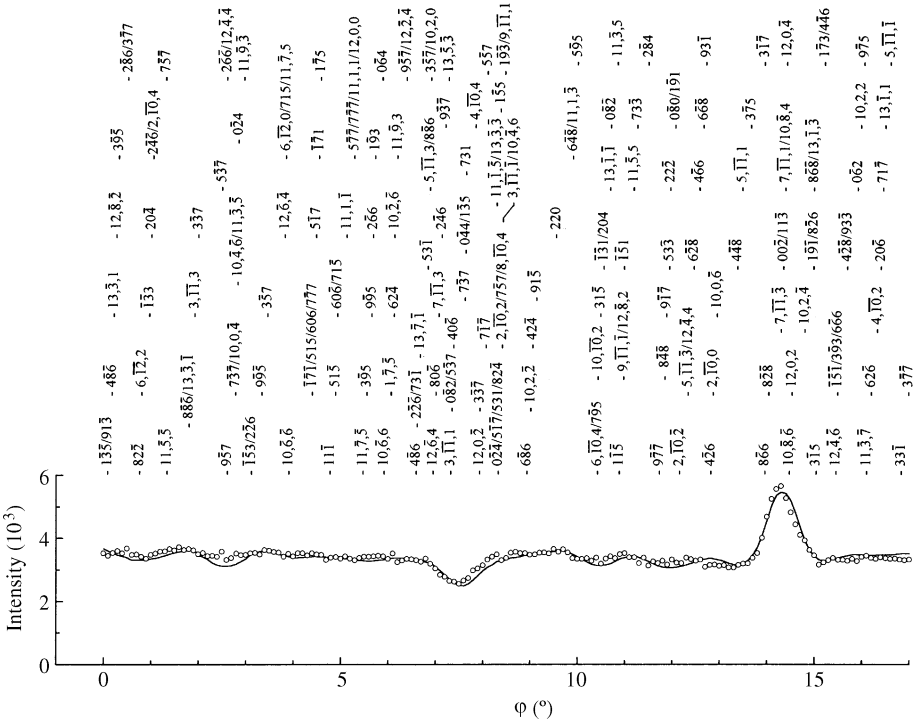

Fig. 4. Indexing of part of the NMD pattern obtained for the paramagnetic phase. Both experimental and simulated patterns are shown. As in Fig. 2, a remarkable high density of secondary reflections is observed.

intrinsically introduce a correction for this phenomenon (Parente *et al.*, 1994). We believe this is the reason why the experimental and simulated NMD patterns exhibit such good agreement as observed in Figs. 1 and 3.

Another point to be noted in the results is that η plays a rather important role in the process of refinement of NMD data. As an experimental parameter, η plays the same role as U, V and W in a refinement by the Rietveld method when a Gaussian function is assumed for the peak shape (Rietveld, 1969; Young, 1991). In theoretical treatments of the multiple diffraction phenomenon, the characteristic mosaic spread of the crystal, which is the standard deviation of the distribution, is given by $\eta = \beta/[2(2\ln 2)^{1/2}]$ where β is the full width at half-maximum (FWHM) of the distribution. In this case, η is an intrinsic value and, as such, is not affected by experimental conditions. On the other hand, in the structural analyses performed in this work, η was considered in a different way. We have verified that, to take into account the effects of beam divergence in the simulations, it is enough to enter into *MULTI* an η value already affected by resolution. To do this, in the formula of η given above, β is substituted by the FWHM of an experimental peak. Therefore, although in our analyses η is still called the mosaic spread, it has lost the characteristic of being an intrinsic parameter and has become one that depends on the particular experiment being performed. At this point, it should be understood that peaks in a multiple diffraction pattern are also enlarged by a geometrical factor (Moon & Shull, 1964; Caticha-Ellis, 1969, 1975; Post, 1975). This factor depends on the inclination of the trajectory described by the reciprocal-lattice point, associated with the secondary reflection producing the peak, with respect to the surface of the Ewald sphere during a φ scan (Rossmanith, 1986). The more inclined the trajectory, the more the peak is enlarged. Although *MULTI* calculates appropriate geometrical factors in order to enlarge peaks in simulated patterns, the inverse procedure, that is, to calculate the *FWHM* of an experimental peak by deconvoluting from it the effect of the geometrical factor, is not feasible, at least in an easy way. For this reason, in refinements I and II we used experimental η values obtained from rocking curves instead of multiple diffraction peaks. The rocking curves were meaured in ω scans carried out in the normal-beam equatorial geometry (Arndt & Willis, 1966) using the same experimental arrangement used in the NMD experiments.

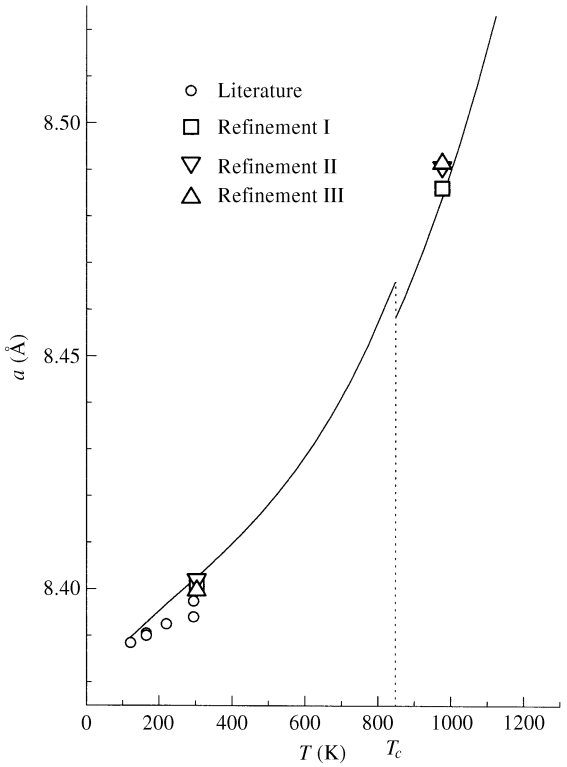

Fig. 5. The consistency of a values found at 926 K in the three refinements of the paramagnetic phase of magnetite. The full lines were calculated according to formulae derived in §6, taking as reference the value $a_0 = 8.402$ Å found at 303 K in refinement II. Results from the literature are: at 122, 165, 220 and 295 K, a = 8.3884, 8.3900, 8.3925 and 8.3974 Å, respectively (Yoshida & Iida, 1979), at 165 and 295 K, a = 8.3905 and 8.3940 Å, respectively (Tombs & Rooksby, 1951), and at 295 K, $a = 0.3940$ Å (Abrahams & Calhoun, 1953).

Although using exactly the same experimental arrangement, the resolution of an ω scan is better than that of a φ scan; *i.e.*, for the same crystal, rocking-curve widths are narrower than multiple diffraction peak widths. This is primarily because a different number of beams are involved in these diffraction phenomena. In the general phenomenon of diffraction $n(n-1)$ interactions occur, n being the number of peaks involved (Parente *et al.*, 1994). The simplest case in multiple diffraction is a three-beam case ($n = 3$). Therefore, a minimum of six interactions occur in multiple diffraction whereas only two interactions occur in single diffraction ($n = 2$). Owing to the larger number of interactions, resolution in multiple diffraction tends to be degenerate compared with single diffraction. We believe this is the reason why, for both phases, the refined η values obtained in refinement III are greater than those (equal) values obtained from rocking curves and used in refinements I and II (see Tables 1 and 2 and the last paragraph in §4, for comparisons).

Another point to be discussed is the fact that the refined η value for one phase is different from that refined for the other phase. As in the Rietveld method where experimental parameters such as U, V and W are refined without any particular attention to the final values, in refinement III η was refined with the sole aim of achieving a better agreement between the experimental and theoretical patterns. Actually, the role played by η in such refinements was to take into account

the effect of beam divergence in the widths of multiple diffraction peaks.

Finally, taking into account the state-of-the-art of the applications of NMD in structural analysis, a few observations are given below.

(*a*) NMD is a single-crystal method and, as such, intensities are affected by extinction. Since neutrons are used in the method, secondary extinction becomes particularly important. It should be noted, however, that the available theory intrinsically corrects the intensities for this phenomenon.

(*b*) Multiple diffraction is a disturbing phenomenon in standard single-crystal diffractometry, particularly when the Ewald sphere is large compared to the reciprocal unit-cell dimensions. In NMD, on the other hand, multiple diffraction causes no disturbing effects since it is the essence of the method.

(*c*) Data acquisition in standard single-crystal diffractometry demands a somewhat complicated procedure involving spatial orientation of the crystal and positioning (2θ) of the detector for each observed reflection. In NMD, except for the φ scan, an experiment is performed in a 'steady state', *i.e.* the crystal and detector are positioned only once.

(*d*) In standard single-crystal diffractometry intensities are, in general, univocally correlated to the square of the structure factor of each reflection. In NMD, on the other hand, this univocal correlation never occurs because of the larger number of beams participating in the phenomenon. In fact, the number of beams involved in the formation of a peak is, in general, very large since all near-neighbour secondary reflections contribute to the intensity of the peak. This is particulary true in an NMD pattern with a high density of secondary reflections (Parente *et al.* 1994).

(*e*) The useful angular extension of a multiple diffraction pattern is limited by the order of the crystallographic axis along the scattering vector of the primary reflection. Lower orders produce more extended patterns.

(*f*) More than one NMD pattern can be used in a structural analysis provided they are obtained with different primary reflections.

Other questions can be posed concerning several other aspects of the NMD method. However, it should be understood this is quite a new method and further study is required.

The authors acknowledge the support of the Conselho Nacional de Desenvolvimento Científico e Tecnológico (CNPq) under contracts Nos. 400397/93-5 and 300136/94-3 (RN), and the International Atomic Energy Agency (IAEA) under research contract No. 6974/RB.

References

Abrahams, S. C. & Calhoun, B. A. (1953). *Acta Cryst.* **6**, 105–106.
Arndt, U. W. & Willis, B. T. M. (1966). *Single Crystal Diffractometry*. Cambridge University Press.
Bacon, G. E. (1975). *Neutron Diffraction*, 3rd ed. Oxford: Clarendon Press.
Buhiya, A. K. & Stanley, E. (1963). *Acta Cryst.* **16**, 981–984.
Caticha-Ellis, S. (1969). *Acta Cryst.* A**25**, 666–673.
Caticha-Ellis, S. (1975). *Jpn. J. Appl. Phys.* **14**, 603–611.
Chang, S.-L. (1984). *Multiple Diffraction of X-rays in Crystals*. Berlin: Springer-Verlag.
Cole, H., Chambers, F. W. & Dunn, H. M. (1962). *Acta Cryst.* **15**, 138–144.
Corliss, L. M., Hastings, J. M. & Brockman, F. G. (1953). *Phys. Rev.* **90**, 1013–1018.
Fleet, M. E. (1986). *J. Solid State Chem.* **62**, 75–82.
Hamilton, W. C. (1958). *Phys. Rev. B*, **110**, 1050–1057.
International Tables for X-ray Crystallography (1974). Vol. IV. Birmingham: Kynoch Press. (Present distributor Kluwer Academic Publishers, Dordrecht.)
Mazzocchi, V. L. & Parente, C. B. R. (1994). *J. Appl. Cryst.* **27**, 475–481.
Moon, R. M. & Shull, C. G. (1964). *Acta Cryst.* **17**, 805–812.
Neel, L. (1948). *Ann. Phys. (Paris)*, **3**, 137–198.
Parente, C. B. R., Mazzocchi, V. L. & Pimentel, F. J. F. (1994). *J. Appl. Cryst.* **27**, 463–474.
Post, B. (1975). *J. Appl. Cryst.* **8**, 452–456.
Rietveld, H. M. (1969). *J. Appl. Cryst.* **2**, 65–71.
Rossmanith, E. (1986). *Acta Cryst.* A**42**, 344–348.
Sharma, S. S. (1950). *Proc. Indian Acad. Sci. Sect. A*, **31**, 261–275.
Shull, C. G., Wollan, E. O. & Koehler, W. C. (1951). *Phys. Rev.* **84**, 912–921.
Tombs, N. C. & Rooksby, H. P. (1951). *Acta Cryst.* **4**, 474–475.
Trueblood, K. N. (1956). *Acta Cryst.* **9**, 359–361.
Verwey, E. J. W. & de Boer, J. H. (1936). *Rec. Trav. Chim. Pays-Bas*, **55**, 531–540.
Verwey, E. J. W. & Haayman, P. W. (1941). *Physica VIII*, **9**, 979–987.
Verwey, E. J. W., Haayman, P. W. & Romeijn, F. C. (1947). *J. Chem. Phys.* **15**, 181–187.
Verwey, E. J. W. & Heilmann, E. L. (1947). *J. Chem. Phys.* **15** (4), 174–180.
Yoshida, J. & Iida, S. (1979). *J. Phys. Soc. Jpn,* **47**, 1627–1633.
Young, R. A. (1991). *The Rietveld Method*. IUCr Monographs on Crystallography 5. Oxford: IUCr/Oxford University Press.